



Damage detection in composite laminates using nonlinear guided wave mixing

Juan Carlos Pineda Allen, Ching Tai Ng ^{*}

School of Civil, Environmental & Mining Engineering, The University of Adelaide, SA 5005, Australia



ARTICLE INFO

Keywords:

Wave mixing
Combined frequency wave
Delamination
Lamb wave
Nonlinear
Composite laminate

ABSTRACT

This paper presents a delamination damage detection technique based on the nonlinear response of Lamb waves in composite laminates. In the approach, a network of transducers is employed to sequentially scan the structure by actuating and receiving dual guided waves. Using combined frequency waves originated due to contact nonlinearity when the incident dual frequency wave interacts with the damage, a damage localization imaging algorithm is proposed to locate the damage and determine the damage location. The proposed damage localization imaging algorithm is based on analysing the cross-correlation of the signal envelope at combined frequency wave with the excitation pulse envelope at incident waves for each transducer pair, the damage localization image is constructed. A numerical study using an experimentally validated finite element model is used to verify the proposed damage detection technique. The results of the numerical study show that, despite the small amplitude of the nonlinear components, the proposed method can effectively predict the damage location, and it does not require baseline measurements, which makes it potential to be a baseline-free damage detection technique.

1. Introduction

Advances in the civil, aerospace and automotive industries have pushed the development of innovative materials that can enhance mechanical properties. However, the development of new materials requires further understanding of their physical properties, as well as their performance and sustainability demands. Composite laminate materials are lightweight, corrosion-resistant, and high-strength materials manufactured with fibres within an epoxy matrix. Despite their excellent mechanical performance in the in-plane direction, composite laminates suffer from relatively weak out-of-plane mechanical properties, which makes them susceptible to delamination defects. Moreover, the in-service operation of composite structural components increases the probability of several types or combinations of damage. Depending on the undertaken task, composite laminate is vulnerable to cracks, fibre breakage, warping, delamination and disbonds, etc. The presence of service-related stresses can further change the degree of damage. Delamination refers to the partial separation between adjoining plies, and can be attributed to manufacturing process defects (e.g. air entrapment) or damage-related mechanisms (e.g. impact) and can derive into poor performance such as loss of carrying capacity [1] or

changed vibration characteristics [2]. Furthermore, delamination is internal and barely visible.

Multiple efforts have been put together within the non-destructive testing (NDT) and structural health monitoring (SHM) communities to address delamination-related damage in composite structures. Non-destructive testing techniques such as eddy current [3], thermography [4], and traditional ultrasonics [5] have shown potential in evaluating this type of damage. Likewise, SHM systems have also been developed using fibre optics [6] and guided waves [7]. Guided waves have been particularly attractive for their ability to inspect long distance, capability to inspect inaccessible areas and low-energy consumption. Moreover, guided waves have the advantage of being suitable for on-site inspection.

Guided waves can be classified as linear guided waves and nonlinear guided waves. Linear guided waves rely on information such as attenuation, reflection, wave velocity and other temporal parameters and have demonstrated effectiveness in detecting damage in composite laminates [8,9]. Nonlinear guided waves rely on nonlinear acoustic phenomena [10]. Its advantage over linear guided waves is they have proven to be more efficient for early damage detection [11], microstructural damage [12], and even undamaged material

* Corresponding author.

E-mail address: alex.ng@adelaide.edu.au (C.T. Ng).

characterization [13]. Recent developments using nonlinear guided waves were achieved using second harmonic generation [14]. Yang *et al.* investigated the second harmonic generation at fatigue crack using low-frequency Lamb waves in isotropic plates [15]. Horizontal cracks due to fatigue damage and impact damage in composites were investigated using second harmonics in [16] and [17] respectively. Soleimanpour *et al.* [18] studied second harmonic generation due to delamination in composites. Temperature-related damage in composites by means of second harmonic generation was also investigated [19]. Nevertheless, second harmonics could also be generated by equipment nonlinearities. The order of magnitude of the second harmonic is often of small magnitude which hinders its extraction for further analysis.

Nonlinear acoustic phenomena can be classified into material nonlinearity and contact nonlinearity. Nonlinear waves have been widely used in the literature to evaluate material nonlinearity due to their advantage to detect micro-scale damage such as dislocations in intact specimens [20,21]. Some studies addressed fatigue damage using bulk waves [22], and others evaluated material nonlinearity using guided waves [23,24], creep damage [11] and plasticity [12] driven damage, which proved efficient for detecting incipient or early stage damage. Contact acoustic nonlinearity (CAN) occurs when the propagating wave induces repetitive collision between the internal surfaces of the damage [25]. It is associated with a stiffness asymmetry at contact-type damage during interaction with the wave. It has been widely investigated for guided wave-based cracks detection in metals [15,26], impact damage in composite laminates [27] and also for bulk waves interaction with damage [28,29].

To overcome the issues of second harmonic generation, mixed-frequency response utilizes two waves of different frequencies to generate combined harmonic waves when the incident waves interact with a source of nonlinearity, either with material or damage-related nonlinearity. Normally known as vibro-acoustic modulation, this approach makes use of a high-frequency probing wave and a low-frequency pumping wave. Early studies explored the potential for material characterization and damage detection [30]. Klepka *et al.* carried out studies to detect cracks [31] and impact damage [32]. Lim *et al.* also conducted extensive research and proposed a field development for crack detection in aluminium plates [33]. The effect of CAN in mixed-frequency response is schematically shown in Fig. 1 for a dual frequency incident wave $x(f_a, f_b)$. During the interaction, the compressive part of the incident wave can travel from one interface to the adjoining interface only during the closure of the damage whereas the discontinuity between interfaces when the damage is open does not allow the wave to pass through, thus generating second and combined harmonics in the output response $y(f_a, f_b, 2f_a, 2f_b, f_{a\pm b})$ of the system. Given the shortcomings of using second harmonic generation such as its small magnitude and equipment-related nonlinearities, combined harmonics will be the attention of this study.

Different to vibro-acoustic modulation, if two high-frequency waves are used the technique is wave-mixing. Researchers have explored the use of bulk wave mixing for the characterization of materials with fatigue and plasticity [34], corroded specimens [35] or thermal aging in adhesive joints [36]. Wave mixing involves two primary waves that interact to generate a secondary wave. In wave mixing problems, wave interactions are classified as co-directional, counter-propagating and non-collinear, depending on the angle of interaction between incident

waves.

More recently, fundamental theoretical and analytical development further enriched the body of literature extending the wave-mixing studies into guided waves [37–39,58,59]. Some studies were carried out to detect different types of damage [40–42].

In the non-collinear wave mixing method, specific mixing angles and mode selection are required for the secondary wave to be generated [39]. Moreover, counter-propagating and non-collinear wave interaction have a smaller mixing zone compared to co-directional wave-mixing. One advantage of co-directional is that the wave mixing zone can be relatively larger and the weakly material nonlinearity can be accumulated [43]. For example, to evaluate material nonlinearity or local fatigue damage the cumulative nature of material nonlinearity was exploited for material characterization or local fatigue through the study of a nonlinearity parameter growth with propagating distance [43–45]. Differently, for contact-type of damage, wave-mixing was used without considering the cumulative influence of material nonlinearity [40,46,47] also reinforcing the benefits of wave mixing. However, there is still much research ahead to take full advantage of and develop in-situ monitoring techniques using guided wave-mixing. As such, this research explores wave-mixing for damage detection and localization in composite laminates.

This study proposes an imaging algorithm for delamination damage detection in a quasi-isotropic laminate. Experimental and finite element studies are conducted to evaluate the proposed technique and the experimentally verified finite element model is used to further investigate the performance of the proposed method.

The paper is organized as follows. Section 1 presented a background of the nonlinear ultrasonic waves due to contact acoustic nonlinearity. The proposed approach for the detection of damage and its localization is presented in Section 2. Next, Section 3 describes the experimental setup, where Lamb wave mode tuning curves, group velocity and displacement amplitude are calculated. Section 4 follows, where a three-dimensional numerical model is described and further validated with experimental results. The imagining algorithm is implemented for various damage locations, and the results and performance are discussed in Section 5. Finally, a conclusion is presented in Section 6.

2. Delamination detection using guided-wave mixing

In the proposed damage detection method, a network of transducers is required to scan the inspected component. Each transducer can be used both as an actuator and sensor for actuating and measuring the signal. The scan is carried out in sequence. When one transducer actuates a dual frequency wave signal $x(f_a, f_b)$, the remaining transducers serve as sensors, which are able to capture the response $y(f_a, f_b, 2f_a, 2f_b, f_{a\pm b})$ in the presence of nonlinearity or $y(f_a, f_b)$ if no damage is present. A four-transducer network is implemented in this study. A representative diagram is shown in Fig. 2a. In the first step, P_1 is the actuator and the signal is received by P_2 , P_3 and P_4 . Following, P_2 is the actuator, and P_1 , P_3 and P_4 are the sensors. This process is sequentially repeated until all four transducers are actuated. When the dual frequency incident wave interacts with the damage, contact nonlinearity is generated and manifested through the existence of combined frequency waves. The signals collected from the network of transducers are expected to contain information regarding the presence and location of the damage. Signals

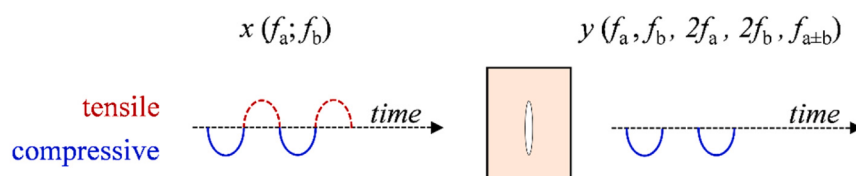


Fig. 1. Schematic representation of the CAN effect in mixed-frequency response.

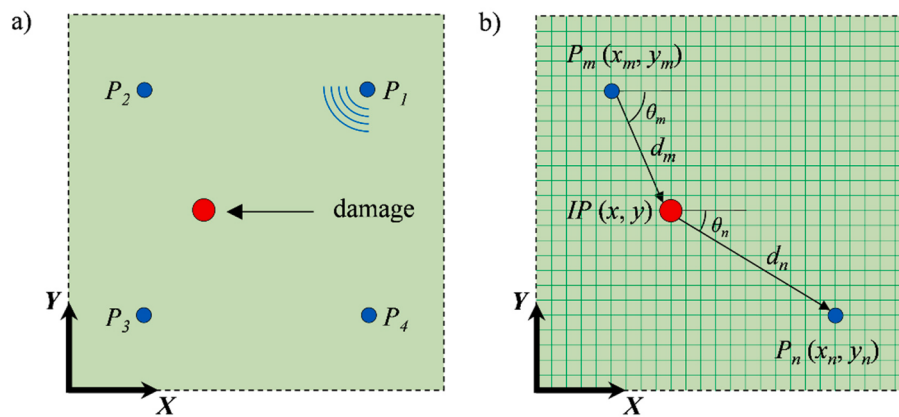


Fig. 2. A) Transducers network actuation and sensing, b) discretization of inspection area for damage image reconstruction.

are recorded for post-processing.

The inspection area is discretised into image pixels (IP) as in Fig. 2b. When the incident dual frequency guided wave interacts with the damage, the combined frequency waves are generated. Under the assumption that the IP is the damage location, the process can be split into two stages: (i) when the incident wave is generated at the transducer \$P_n\$, propagates and arrives at the IP \$(x, y)\$ and (ii) when the combined frequency wave is generated at the IP (assumed damage location) and propagates to the transducer \$P_m\$. Locations of the transducers and IP are known before carrying out the inspection. The group velocity (\$c_{gr}\$) values for the incident waves are obtained experimentally and numerically, and their values are presented in Sections 3.4 and 4.2, respectively. The group velocities corresponding to the combined frequency waves are calculated numerically. They are not included in this paper for the sake of brevity. To calculate the arrival time of the combined frequency wave:

$$t_{mn}(x, y) = \frac{\sqrt{(x - x_m)^2 + (y - y_m)^2}}{c_g^{fi}(\theta_m)} + \frac{\sqrt{(x_n - x)^2 + (y_n - y)^2}}{c_g^{fc}(\theta_n)} \quad (1)$$

where \$x_m\$ and \$y_m\$ are the coordinates of the actuator and \$x_n\$ and \$y_n\$ are the coordinates of the sensor as shown in Fig. 2. The first term on the right-hand side of Eq. (1) is the arrival time of the incident frequency wave from transducer \$P_n\$ to the image pixel IP \$(x, y)\$ and the second term is the arrival time of the combined frequency wave from the image pixel IP \$(x, y)\$ to the transducer \$P_m\$. The average value of the group velocities of the incident frequencies is \$c_g^{fi}(\theta_m)\$ and \$c_g^{fc}(\theta_n)\$ is the group velocity of the combined frequency wave. Given that the structural component under study is not perfectly isotropic, group velocity values are angular dependent, indicated by \$\theta_m\$ for the propagation direction between the actuator and the damage, and \$\theta_n\$ for the propagation direction between the damage and the sensor.

A time-frequency analysis using a short-time Fourier transform is carried out to extract data corresponding to the incident frequency and those corresponding to the combined frequency waves. Cross-correlation between the incident pulse actuated at \$P_n\$ and the measured signal at \$P_m\$ is carried out in this study. It is defined as:

$$C_{mn}(t) = \int_0^T A_{mn}\left(\tau, f_{\frac{a+b}{2}}\right) S_{mn}(t + \tau, f_{a \pm b}) \quad (2)$$

where \$A_{mn}\$ is the averaged time-frequency data of the actuated pulse at frequencies \$f_a\$ and \$f_b\$. \$S_{mn}\$ is the time-frequency data of the scattered pulse at combined frequencies \$f_{a \pm b}\$, when \$P_m\$ and \$P_n\$ are actuator and sensor, respectively. In this study, the cross-correlation between the time-frequency data at the incident frequencies and time-frequency data at combined frequency is used to determine the time shift for describing the source location of the combined frequency harmonic.

When the dual-frequency incident pulse is sent from transducer \$m\$, the time-frequency data of the actuated signal is obtained by using STFT. Given there are two frequencies in the incident pulse, the average value of time-frequency data is obtained as \$A_{mn}\$. The received signal by actuator \$n\$ contains harmonics corresponding to the dual-frequency incident pulse and combined harmonics which originated due to the contact effect. The time-frequency data of this received signal is also obtained using STFT, as \$S_{mn}\$. Then, by superimposing the power flux of all the actuator-sensor path images [48], the damage detection is reconstructed as:

$$I(x, y) = \sum_{m=1}^N \sum_{n \neq m}^N \beta_{mn} (C_{mn}(t_{mn}))^2 \quad (3)$$

where \$\beta_{mn}\$ is a factor that takes into consideration the varying sensitivities for each signal path of the image. To ensure the damage detection is practical for development and implementation small and inexpensive piezoceramic transducers, instead of the SLDV used in Section 3.2, are employed.

3. Experiment

This section provides detailed descriptions of the experimental setup, which includes the composite laminate specimen, and the actuators and sensors.

3.1. Specimen description

A composite laminate with in-plane dimensions of \$800 \text{ mm} \times 800 \text{ mm}\$ was manufactured using eight layers of unidirectional carbon/epoxy Eporite EHM-32 prepreg lamina with stacking sequence [-45/45/0/90]\$_S\$. The fibre volume fraction is 0.55, the density is \$1300 \text{ kg/m}^3\$ density, and the thickness is 0.25 mm. The total thickness of the composite laminate is 2.00 mm. The elastic properties of the lamina are listed in Table 1.

3.2. Actuating and sensing

The guided wave was excited by an adhesively bonded piezoceramic transducer with 5 mm diameter and 2 mm thickness bonded with epoxy adhesive to the composite laminate. A 3 mm thick and 5 mm diameter

Table 1
Elastic properties of the lamina.

\$E_{11}\$ (GPa)	\$E_{22} = E_{23}\$ (GPa)	\$G_{12} = G_{13}\$ (GPa)	\$G_{23}\$ (GPa)	\$\nu_{12} = \nu_{13}\$	\$\nu_{23}\$
111	7.16	3.62	2.20	0.33	0.44

brass backing mass was similarly bonded on top of the piezoceramic transducer with silver conductive epoxy (to couple mechanically and electrically to the piezoceramic transducer) to increase the out-of-plane excitability. Wires were soldered on top of the backing mass and onto a terminal bonded to the composite laminate. A traditional BNC female connector was used. To conduct the guided wave experiments in this section, an actuating and sensing system was employed in this study. The system, which consists of a computer-controller arbitrary waveform generator, a power amplifier and a Scanning Laser Doppler Vibrometer (SLDV), is schematically shown in Fig. 3. The angle between the laser beam and the specimen surface is α .

3.3. Mode-tuning curve

A mode-tuning analysis was first carried out to determine the excitability of both the anti-symmetric (A_0) and symmetric (S_0) Lamb wave modes at different excitation frequencies. A 5-cycle sinusoidal tone burst pulse modulated by Hann window was created by the computer-controller arbitrary function generator and amplified up to 160Vpp and then sent to the piezoceramic transducer. The generated Lamb waves range from 60 kHz to 400 kHz in steps of 20 kHz are measured using a one-dimensional laser scan, with the laser head positioned at $\alpha = 30^\circ$ angle with respect to the specimen surface such as the laser beam out-of-plane sensitivity can capture both the S_0 and A_0 modes. The amplitude of the wave was measured using the displacement component of data captured by the SLDV. A fixed location 100 mm away from the transducer in the $\theta = 0^\circ$ direction of the composite plate orientation is chosen for measurement. Preliminary tests indicated that A_0 mode is separated from S_0 mode at the selected distance. A low-pass filter and averaging are used in the acquisition of the data. The obtained mode tuning curve is shown in Fig. 4. For the purpose of the studies, we can see that the amplitude of the A_0 mode is reasonably larger than the S_0 for a frequency band ranging from 140 to 280 kHz. In the literature, it has been widely reported that the S_0 cannot be used for detecting the delamination at the through-thickness locations with zero shear stress [49] while the A_0 is sensitive to the delamination at all through-thickness locations [8,50]. Hence, in this study, the A_0 is used as the excited wave in the delamination detection.

3.4. Amplitude, group velocity and frequencies selection

Based on the obtained mode tuning curve from the previous section, a number of preliminary tests were conducted in order to determine a suitable frequency pair for the damage detection studies. Given its sensitivity and dominant out-of-plane displacement, the two frequencies should have similar excitability of the A_0 mode, and the chosen frequency pair is 170 kHz and 250 kHz. In addition, the combined harmonic of this frequency pair is not a multiple of the incident wave frequency as this could help distinguish the second harmonics from the combined harmonics in the frequency domain. The tests of this section were carried out to calculate group velocity and amplitude values of the

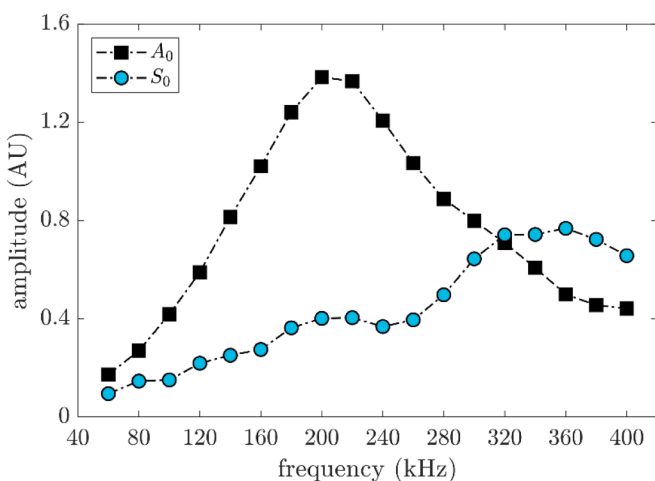


Fig. 4. Mode tuning curve at $\theta = 0^\circ$.

A_0 mode. The measurements of this section were conducted using a SLDV with the laser head positioned at $\alpha = 90^\circ$ angle, such as the laser beam is perpendicular to the surface of the composite plate. This setup allows flexibility to scan many points using non-contact sensing. Out-of-plane displacement was obtained for 36 points, at 10° from each other and located at $r = 80$ mm from the centre of the piezoceramic transducer, another 36 points at $r = 90$ mm and 36 more points at $r = 120$ mm. In total, the scan comprised 108 points. A 6-cycle 170 kHz tone burst pulse was created using an arbitrary waveform generator and sent to a power amplifier. The signal was amplified up to 160Vpp and fed to the piezoceramic transducer. The signal acquisition was averaged 1,000 times to minimize the noise effect and filtered using a low-pass filter. Similar experiments were also conducted for a 6-cycles 250 kHz tone burst pulse.

3.5. Combined frequency

In addition to the amplitude and group velocity studies, in order to experimentally investigate the combined harmonic generation an identical composite plate was manufactured as in Section 3.1. However, to create the delamination damage, a 15 mm diameter and 0.05 mm thick Teflon film was inserted during the lay-up process between the third and fourth layer of the composite plate, which is asymmetrically located in the thickness direction of the composite laminate. Teflon sheet insert has been widely used in the literature for the purpose of creating artificial delamination damage in composite laminates. A pitch-catch configuration with adhesively bonded piezoceramic transducers with 5 mm diameter and 2 mm thickness with 3 mm thick and 5 mm diameter backing mass was used and arranged in the 0° direction of the quasi-isotropic plate. The distance between the transducers was 150 mm from each other. A similar configuration was set up for the plate with no

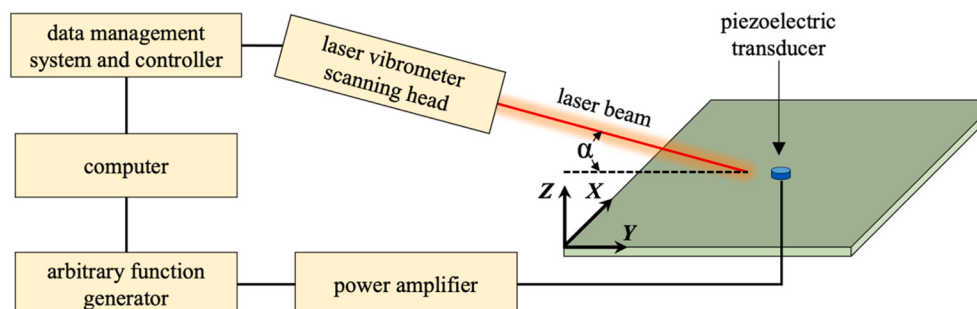


Fig. 3. Experimental configuration.

delamination.

4. Three-dimensional explicit finite element simulation

4.1. Model description

To simulate the guided wave propagation in the quasi-isotropic composite laminate, a three-dimensional finite element (FE) model is developed using ABAQUS software. The dimension of the model is $375 \times 375 \times 2 \text{ mm}^3$. Each of the 8 plies is modelled as a unidirectional layer and orientated according to the stacking sequence $[-45/45/0/90]_S$, and tied with its corresponding top and bottom layer using tie constraints. Eight-noded solid brick elements with reduced integration were used. The maximum element size was set to be $0.20 \times 0.20 \times 0.25 \text{ mm}^3$. There is one element through the thickness of each ply and there are 8 layers of elements in the thickness direction of the composite laminate. To avoid wave reflections from the edge, absorbing layers by increased damping (ALID) are modelled all around the four sides of the plate [51]. There are 50 layers in total, each layer is 1 mm wide. Thus, the total width of the absorbing layer is 50 mm and the dimension of the plate without ALID is $275 \times 275 \text{ mm}^2$. Mass-proportional damping was used in ALID. The power-law formulation in Eq. (4) calculates the value of damping at each layer.

$$\varphi_M(x) = \varphi_{\max} \times Y(x)^P \quad (4)$$

where the location from the edge of the plate to a location of ALID is indicated by x . In the study, $P = 3$ and $\varphi_{\max} = 250,000$.

A_0 mode Lamb wave is excited by applying out-of-plane displacement to a circular area of 5 mm diameter and centered at ($x = 187.5\text{mm}$; $y = 187.5\text{mm}$), which is the same area covered by the piezoelectric disc transducer in the experiment as described in Section 3.2. Out-of-plane displacement was obtained for 36 points located at $r = 80 \text{ mm}$ from the centre of the excitation area, another 36 points at $r = 90 \text{ mm}$ and 36 additional points at $r = 120 \text{ mm}$, as shown in Fig. 5.

4.2. Amplitude and group velocity

A typical numerically simulated time domain signal with its corresponding frequency spectra is shown in Fig. 6 together with the

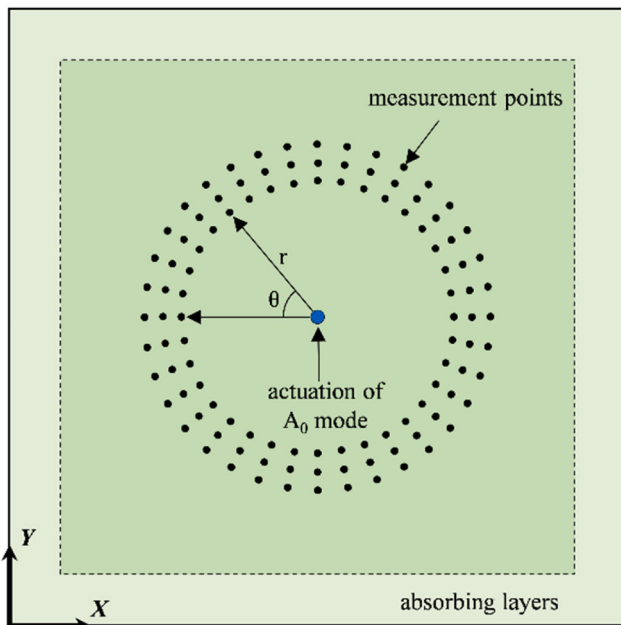


Fig. 5. Schematic diagram of the FE model with actuation and sensing points.

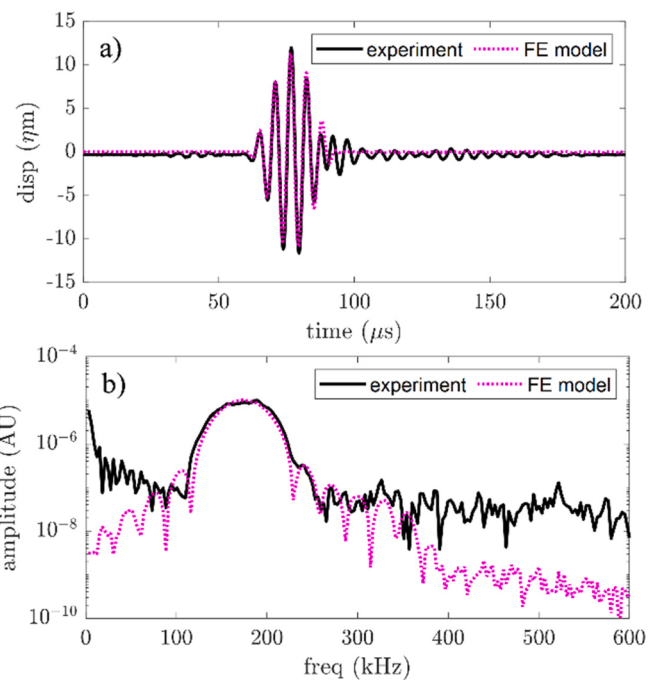


Fig. 6. Typical a) time domain, and b) frequency domain data for a point located at $r = 80 \text{ mm}$ and $\theta = 0^\circ$ from the actuator.

experimental data, which was measured at the location $r = 80 \text{ mm}$ from the centre of the actuator and $\theta = 0^\circ$ of the composite plate. The excitation is 170 kHz. Further, normalized displacements and group velocity were calculated and are shown in Fig. 7. Group velocity was calculated using the envelope of the time domain signal and the distance between consecutive points for all values of θ . Normalized displacements were calculated for 36 points located at $r = 80 \text{ mm}$ from the actuator. An offset in the group velocity is observed in Fig. 7a and Fig. 7b. In general, group velocity values measured experimentally are slightly larger than group velocity values measured numerically. The largest difference for the 170 kHz pulse exists at the 210° direction, where group velocity is 1379 m/s for the numerical model and 1559 m/s for the experiment. For the 250 kHz pulse, the largest difference exists at 320° , where group velocity is 1397.48 m/s for the numerical model and 1572 m/s for the experiment. Conversely, the smallest difference for the 170 kHz pulse exists at 60° , where group velocity values are 1401 m/s and 1410 m/s for the numerical model and experiment respectively. Likewise, for the 250 kHz pulse, the smallest difference exists at the 30° direction, with 1379 m/s and 1359 m/s values for the numerical model and experiment respectively. This difference was quantified for all the group velocity values. The mean differences in the group velocity values are around 6.3 % for the 170 kHz pulse and 6.8 % for the 250 kHz pulse. For the purpose of this study, the offset is not significant which can be later reflected in the accuracy of the results.

Furthermore, since a dual frequency approach is employed in this study, the velocities at which the pulses at different frequencies propagate were also evaluated and are shown in Fig. 8. For the experimentally measured data in Fig. 8a, the maximum difference exists at the 30° direction with the 170 kHz pulse propagating 12.2 % faster than the 250 kHz pulse. In contrast, the minimum difference was at the 150° direction with the 250 kHz pulse propagating at 0.1 % faster than the 170 kHz pulse. For the numerical case scenario in Fig. 8b, the maximum difference was found to be at the 310° direction with the 170 kHz pulse propagating 3.8 % faster than the 250 kHz pulse and the minimum difference at the 220° direction with the 250 kHz pulse propagating at a 0.1 % faster than the 170 kHz pulse. It has been shown that the effect of the group velocity difference is mainly in the interaction zone, and thus

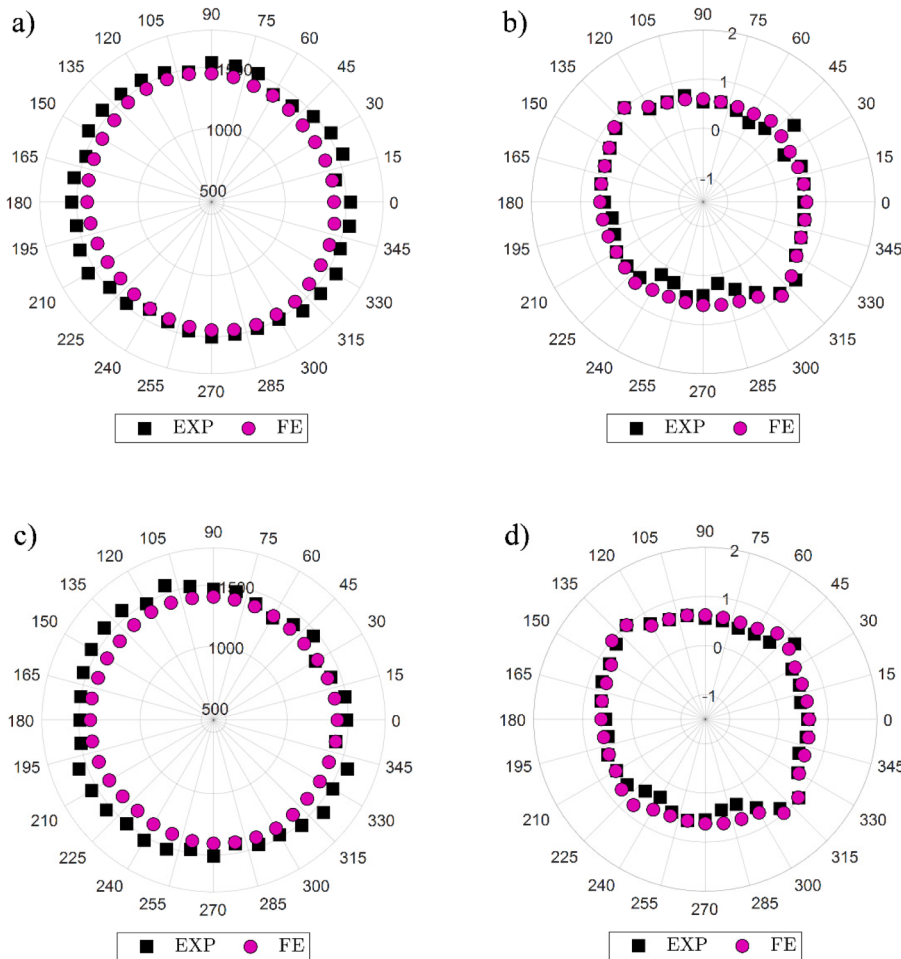


Fig. 7. A) Group velocity 170 kHz pulse, b) normalized amplitude 170 kHz pulse, c) group velocity 250 kHz pulse, and d) normalized amplitude 250 kHz pulse.

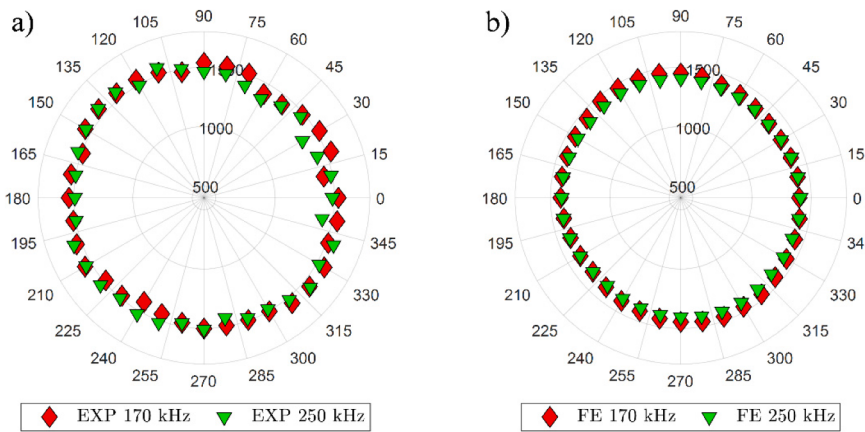


Fig. 8. A) Group velocity 170 kHz and 250 kHz pulses for experimental data, and b) group velocity 170 kHz and 250 kHz pulses for numerical data.

in the amplitude of the secondary wave [45]. Nevertheless, approximate group velocity via dual frequency approach was demonstrated effective for collinear wave mixing [41,40]. Therefore, based on the time domain and frequency domain data, together with the group velocity and normalized amplitude, it can be concluded that the FE model can accurately predict Lamb wave propagation.

4.3. Combined frequency

Two corresponding numerical models to the experimental setup in Section 3.5 were developed. Identical stacking sequence, mesh element size and material properties as described in Section 4.1 were used. In one of the models, a 15 mm-diameter delamination is introduced in the model by relaxing the tie constraints between the third and the fourth layer of the composite laminate. To avoid interpenetration between untied surfaces so that the CAN effect can be simulated a hard contact

and surface-to-surface contact interaction is implemented in the FE model. The layers of the undamaged model were left fully tied. A dual frequency signal A_0 mode Lamb wave is excited as in [Section 4.1](#). Out-of-plane displacement was obtained for a point located at 150 mm in the $\theta = 0^\circ$ of the composite plate.

In the interest of investigating the combined harmonic generation, the frequency domain response for the experiments and corresponding numerical simulations is shown in [Fig. 9](#). It can be seen, that apart from the incident waves, the combined frequency waves are generated as a result of the contact effect in the delaminated specimen and FE model, whereas they do not show in the undamaged specimen and corresponding FE model. It is also noted that the amplitudes of the nonlinear components are smaller, by a factor of approximately 450 for the difference frequency harmonic and a factor of approximately 80 for the sum frequency harmonic, than the amplitude of the linear components. Previous studies have reported that the difference could be one [40,52], two [53] or up to three [45,54] orders of magnitude differences depending on the excitation frequencies, specimens and wave modes used in the studies. In addition to the amplitude and arrival time, the FE model is also validated against the combined harmonic generation.

5. Finite element studies

To implement the proposed damage detection technique, a series of finite element simulations were conducted. The model is similar to the validated finite element model described in [Section 4.1](#) in terms of stacking sequence, mesh element size and material properties. However, for the purpose of the studies of this section, a four-transducer network and a delamination damage were introduced. Coordinates of the transducers are $x_{P1} = 212.5\text{mm}$, $y_{P1} = 212.5\text{mm}$; $x_{P2} = 62.5\text{mm}$, $y_{P2} = 212.5\text{mm}$; $x_{P3} = 62.5\text{mm}$, $y_{P3} = 62.5\text{mm}$ and $x_{P4} = 212.5\text{mm}$, $y_{P4} = 62.5\text{mm}$. Building upon the selection of the frequencies in [Section 3.4](#), in the present studies each transducer is excited sequentially using a dual frequency incident signal while the rest of the transducers are used as the sensors. A dual frequency signal A_0 mode Lamb wave is excited as in [Section 4.1](#). Three different damage locations were evaluated and are listed in [Table 2](#). A 15 mm-diameter delamination is introduced in the model between the third and fourth layer of the composite laminate. Hard contact and surface-to-surface contact interaction are implemented in the FE model as in [Section 4.3](#).

A contact effect is expected when the dual-frequency incident wave interacts with the damage. As a result, the signals received in the remaining transducers contain fundamental frequencies and combined frequencies, which are due to contact nonlinearity, as shown in [Fig. 9](#).

Given that the proposed damage detection technique requires time–frequency data, special attention is necessary when selecting the number of windows. The number of windows has effect on the resolution of the frequency domain of the time–frequency data. In this study, Hann window was used. A typical spectrogram, or time–frequency analysis is

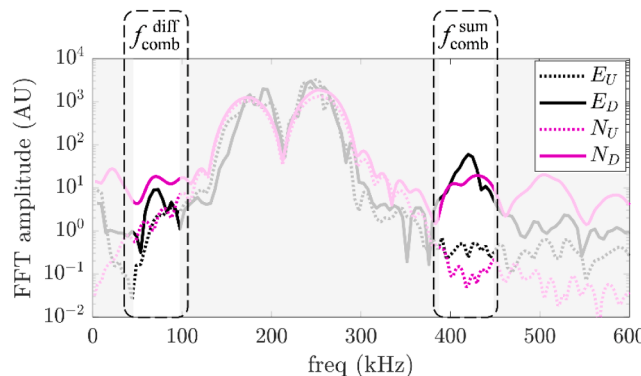


Fig. 9. Combined harmonic generation for experimental and numerical studies.

Table 2

Damage location coordinates in each damage case.

	x_d (mm)	y_d (mm)
Case A	187.5	147.5
Case B	232.5	92.5
Case C	87.5	107.5

shown in [Fig. 10a](#)-10b) for Case C when P_1 is excited and the signal is received by P_2 , the incident frequencies and combined frequency wave are observed. For this case, the total number of windows is $n_w = 6$.

Once the sequential scan process is completed, all the signals are collected and processed using the time–frequency analysis, then signals are extracted as shown in [Fig. 10b](#). With this information, each actuator–sensor contributes to the total reconstructed image. By using Equation (3), and the combined frequency wave at the sum frequency harmonic, the reconstructed image for Case A is shown in [Fig. 11a](#)-11b), for two different numbers of windows n_w . Using the combined frequency wave at the difference frequency harmonic, a similar image can also be also reconstructed as in [Fig. 11c](#)-11d). To provide a more robust image location of the damage, a binary image is created by filtering out minor intensity peaks of the reconstructed image using an arbitrary threshold value [55]. In this study, a threshold value of 85 % is used. The centroid of the binary image is calculated (indicated with a cross mark) and compared to the centroid of the actual damage (indicated with a hollow black circle). The location of the transducers is marked with a white circle. To quantify the error between the estimated damage location and actual damage location, an error is defined as $\text{Err} = \sqrt{(x_e - x_r)^2 + (y_e - y_r)^2}$, which is indicated for each of the binary images from the reconstructed images. It is observed that for Case A shown in [Fig. 11a](#) and 11d), for $n_w = 6$, detection error is less for the reconstructed images using combined frequency wave at difference frequency harmonic, however as the number of windows increased the error was observed to favourably decrease using combined frequency wave at sum

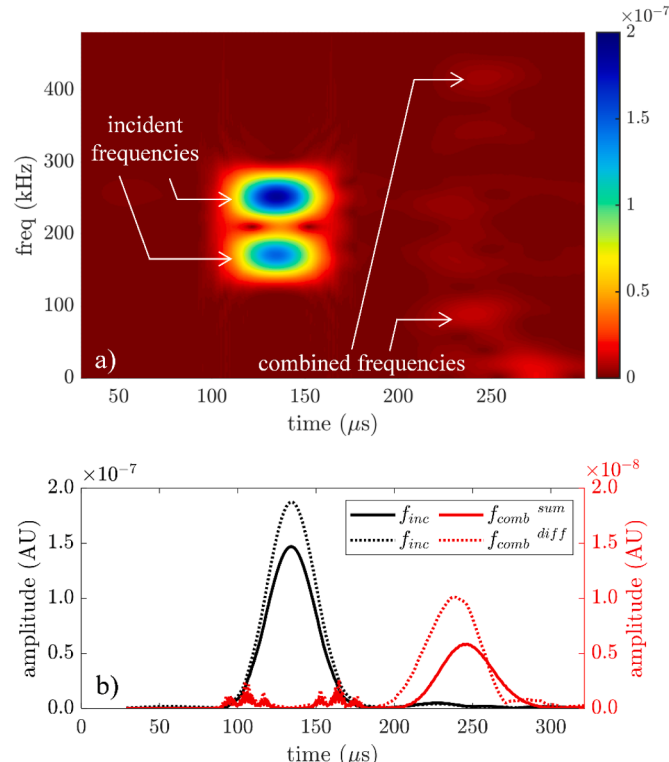


Fig. 10. A) Spectrogram for the signal actuated by P_1 and received by P_2 and, b) corresponding time–frequency data for the harmonics of interest.

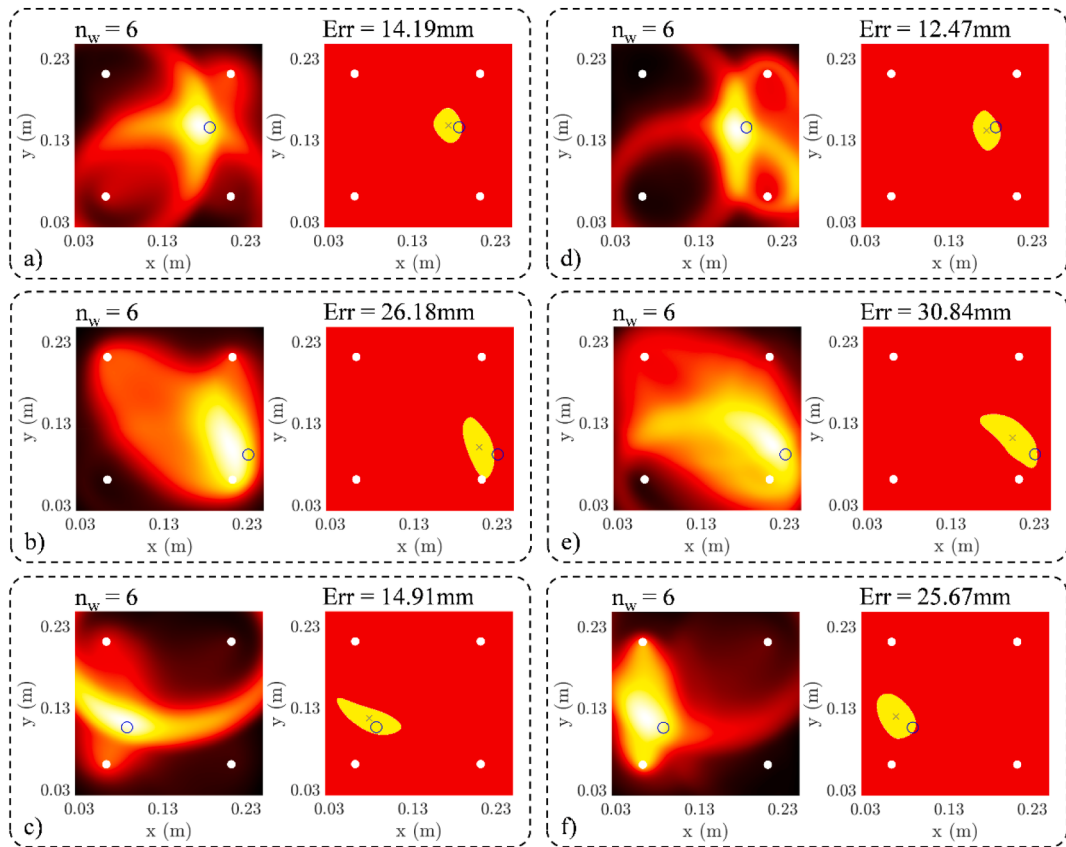


Fig. 11. Reconstructed images and binary images of the estimated damage location using $n_w = 6$ for a) Case A with combined frequency wave at sum frequency, b) Case B with combined frequency wave at sum frequency, c) Case C with combined frequency wave at sum frequency, d) Case A with combined frequency wave at difference frequency, e) Case B with combined frequency wave at difference frequency, and f) Case C with combined frequency wave at difference frequency (hollow circle: actual damage location, cross: predicted damage location).

frequency harmonic. In Case B (where the damage is located outside of the transducer network area) shown in Fig. 11b and 11e), the error is lesser using the sum frequency harmonic as compared to the difference frequency harmonic, although the performance of the imaging algorithm seems to be slightly reduced. Similarly for Case C results shown in Fig. 11c and 11f), the error is greater, by almost two times, using the difference frequency harmonic.

The performance under different window numbers was evaluated. It was found that while increasing the window number, the detection error for Case A using the combined frequency wave at the sum frequency harmonic steadily decreases. But its counterpart using the difference frequency harmonic decreases at the beginning reaching a plateau and then the error increases. For Case B, detection error with the use of the sum frequency harmonic outperforms the use of the difference frequency harmonic, although the errors trend to equalize around $n_w = 7$. For Case C, both detection errors show a similar decreasing trend but the use of the sum frequency harmonic does also surpass the use of the difference frequency harmonic. Consideration must be paid while reducing the error by increasing the number of windows, as some frequency information could be neglected if the number of windows is increased indefinitely. Using the wave mixing approach possesses the advantage that it is a potentially baseline-free approach. Moreover, the wave mixing approach can avoid equipment nonlinearities, which is an issue for second harmonic approaches.

Fig. 12 compares the effect of the number of windows for each of the cases. It is observed that by using the sum frequency harmonic, the damage detection technique is more robust than using the difference frequency harmonic. One possible reason is that in general, the extracted time-frequency signals from the sum frequency harmonic are more evident as compared to the difference frequency harmonic for the

selected frequencies in this study. The authors believe this effect is due to the magnitude of the difference frequency harmonic, its bandwidth and how separated it is from the incident frequency harmonics. Even though the performance of the proposed approach can be by some means constrained when the damage is located outside of the transducer network as in case B, the number of windows between 6 and 8 would ideally provide better results with the least error for all the evaluated damage locations and without compromising the resolution of the time-frequency data. Special attention must be paid while increasing the number of windows to reduce the error, as a significant increase in the number of windows would potentially cause some frequency information to be omitted.

It was observed that the amplitudes of the nonlinear components are smaller than the amplitude of the linear components for both the experimental and numerical results. Previous studies have reported that the difference could be one [40,52], two [53] and up to three [45,54] orders of magnitude difference depending on the excitation frequencies, specimens and wave modes used in the studies. Although there are a variety of advantages of using the nonlinear components of ultrasonic guided waves such as high sensitivity to early-stage and small defects and the potential to be a baseline-free damage detection technique, the relatively low amplitude of the nonlinear components is still a disadvantage of the nonlinear ultrasonic guided wave approach. To practically apply this technique, researchers have proposed techniques to more robustly extract the nonlinear components from the measurements, e.g. using the phase reversal approach [56,57], and minimise the non-damage related nonlinear components generated by the equipment nonlinearity, e.g. using the wave mixing approach with two individual excitation sources.

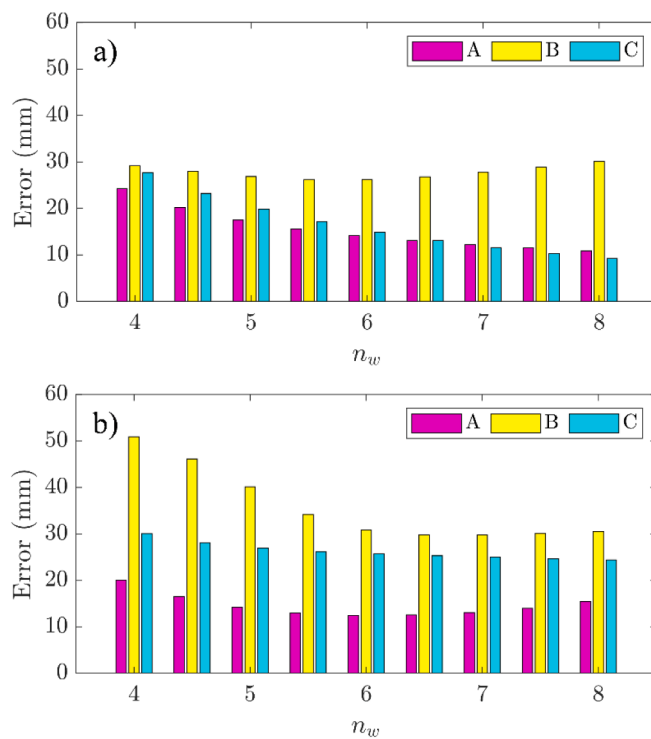


Fig. 12. Relationship between error and number of windows when using combined frequency wave at a) Sum frequency harmonic and b) Difference frequency harmonic.

6. Conclusions

A baseline-free delamination damage detection in composite laminates using nonlinear combined frequency waves has been proposed in this paper. The proposed approach employs a time–frequency analysis and the combined frequency wave generated due to contact nonlinearity at the damage. Several damage cases with different damage locations have been investigated both within and beyond the area enclosed by the transducer network. The effect of the number of windows in the time–frequency analysis has been investigated and demonstrated that for the cases studied in this paper, employing the sum harmonic frequency could provide more robust results, although there are some limitations if the damage is located outside of the transducer network. Moreover, the time–frequency analysis in the proposed approach allows extraction of the signals without relying on baseline data and paves the way for in-situ damage localization and monitoring techniques as it has the potential to be implemented using multiplexing technology in the data acquisition system. The study in this paper is a first step toward the practical application of using the guided wave mixing approach for delamination detection in composite laminates. The study has demonstrated the guided wave mixing technique can be applied to composite laminates, in which wave velocities at each propagation direction are different. The results of the numerical study using the experimentally verified FE model show that the wave mixing approach can be used to determine the delamination location in composite laminates even there is a reasonable level of group velocity mismatching. To address the relatively small amplitude of the nonlinear components, future work will focus on investigating the robustness of extracting the nonlinear components in guided wave mixing.

CRediT authorship contribution statement

Juan Carlos Pineda Allen: Conceptualization, Methodology, Software, Validation, Formal analysis, Writing – original draft. **Ching Tai Ng:** Conceptualization, Supervision, Writing – review & editing.

Declaration of Competing Interest

The authors declare that they have no known competing financial interests or personal relationships that could have appeared to influence the work reported in this paper.

Data availability

Data will be made available on request.

Acknowledgment

This work was funded by the Australia Research Council (ARC) under grant numbers DP200102300 and DP210103307. J.C. Pineda Allen is grateful for the scholarship support received from Endeavour Leadership Program. The supports are greatly appreciated.

References

- [1] İpek G, Arman Y, Çelik A. The effect of delamination size and location to buckling behavior of composite materials. *Compos B Eng* 2018;155:69–76.
- [2] Klepka A, et al. Impact damage detection in composite chiral sandwich panels using nonlinear vibro-acoustic modulations. *Smart Mater Struct* 2013;22(8):084011.
- [3] He Y, et al. Non-destructive testing of low-energy impact in CFRP laminates and interior defects in honeycomb sandwich using scanning pulsed eddy current. *Compos B Eng* 2014;59:196–203.
- [4] Addepalli S, et al. Non-destructive evaluation of localised heat damage occurring in carbon composites using thermography and thermal diffusivity measurement. *Measurement* 2019;131:706–13.
- [5] Nesijski E. Some aspects of ultrasonic testing of composites. *Compos Struct* 2000; 48(1):151–5.
- [6] Jang B-W, Kim C-G. Real-time detection of low-velocity impact-induced delamination onset in composite laminates for efficient management of structural health. *Compos B Eng* 2017;123:124–35.
- [7] Mei H, et al. Vibration-Based In-Situ Detection and Quantification of Delamination in Composite Plates. *Sensors* 2019;19(7):1734.
- [8] Ramadas C, et al. Interaction of guided Lamb waves with an asymmetrically located delamination in a laminated composite plate. *Smart Mater Struct* 2010;19 (6):065009.
- [9] Su Z, Ye L. Fundamental Lamb Mode-based Delamination Detection for CF/EP Composite Laminates Using Distributed Piezoelectrics. *Struct Health Monit* 2004;3 (1):43–68.
- [10] Jhang KY. Nonlinear ultrasonic techniques for nondestructive assessment of micro damage in material: A review. *Int J Precis Eng Manuf* 2009;10(1):123–35.
- [11] Xiang Y, et al. Effect of precipitate-dislocation interactions on generation of nonlinear Lamb waves in creep-damaged metallic alloys. *J Appl Phys* 2012;111 (10):104905.
- [12] Pruell C, et al. A nonlinear-guided wave technique for evaluating plasticity-driven material damage in a metal plate. *NDT and E Int* 2009;42(3):199–203.
- [13] Bermes C, et al. Experimental characterization of material nonlinearity using Lamb waves. *Appl Phys Lett* 2007;90(2):021901.
- [14] Matlack KH, et al. Review of Second Harmonic Generation Measurement Techniques for Material State Determination in Metals. *J Nondestr Eval* 2014;34 (1):273.
- [15] Yang Y, et al. Second harmonic generation at fatigue cracks by low-frequency Lamb waves: Experimental and numerical studies. *Mech Syst Sig Process* 2018;99: 760–73.
- [16] Rauter N, Lammering R, Kuhnrich T. On the detection of fatigue damage in composites by use of second harmonic guided waves. *Compos Struct* 2016;152: 247.
- [17] Rauter N, Lammering R. Impact Damage Detection in Composite Structures Considering Nonlinear Lamb Wave Propagation. *Mech Adv Mater Struct* 2015;22 (1–2):44–51.
- [18] Soleimaniour R, Ng CT. Locating delaminations in laminated composite beams using nonlinear guided waves. *Eng Struct* 2017;131:207–19.
- [19] Li W, Cho Y, Achenbach J. Detection of thermal fatigue in composites by second harmonic Lamb waves. *Smart Mater Struct* 2012;21(8):085019.
- [20] Yeung C, Ng CT. Nonlinear guided wave mixing in pipes for detection of material nonlinearity. *J Sound Vib* 2020;485:115541.
- [21] Broda D, et al. Modelling of nonlinear crack-wave interactions for damage detection based on ultrasound—A review. *J Sound Vib* 2014;333(4):1097–118.
- [22] Cantrell J, Yost W. Nonlinear ultrasonic characterization of fatigue microstructures. *Int J Fatigue* 2001;23:487–90.
- [23] Deng M, Pei J. Assessment of accumulated fatigue damage in solid plates using nonlinear Lamb wave approach. *Appl Phys Lett* 2007;90(12):121902.
- [24] Bermes C, et al. Nonlinear Lamb waves for the detection of material nonlinearity. *Mech Syst Sig Process* 2008;22(3):638–46.
- [25] Solodov IY, Krohn N, Busse G. CAN: an example of nonclassical acoustic nonlinearity in solids. *Ultrasonics* 2002;40(1):621–5.

- [26] Yelva N, Mira M, Mujumdar P. Spectral damage index for estimation of breathing crack depth in an aluminum plate using nonlinear Lamb wave. *Struct Control Health Monit* 2014;21(5):833–46.
- [27] Shkerdin G, Glorieux C. Nonlinear clapping modulation of lamb modes by normally closed delamination. *IEEE Trans Ultrason Ferroelectr Freq Control* 2010;57(6):1426–33.
- [28] Biwa S, Nakajima S, Ohno N. On the Acoustic Nonlinearity of Solid-Solid Contact With Pressure-Dependent Interface Stiffness. *J Appl Mech* 2004;71(4):508–15.
- [29] Yan D, Drinkwater BW, Neild SA. Measurement of the ultrasonic nonlinearity of kissing bonds in adhesive joints. *NDT and E Int* 2009;42(5):459–66.
- [30] Donskoy D, Sutin A. Vibro-Acoustic Modulation Nondestructive Evaluation Technique. *J Intell Mater Syst Struct* 1998;9(9):765–71.
- [31] Klepka A, et al. Nonlinear acoustics for fatigue crack detection – experimental investigations of vibro-acoustic wave modulations. *Struct Health Monit* 2012;11(2):197–211.
- [32] Klepka A, et al. Impact damage detection in laminated composites by non-linear vibro-acoustic wave modulations. *Compos B Eng* 2014;65:99–108.
- [33] Lim HJ, et al. Development and field application of a nonlinear ultrasonic modulation technique for fatigue crack detection without reference data from an intact condition. *Smart Mater Struct* 2016;25(9):095055.
- [34] Croxford A, et al. The use of non-collinear mixing for nonlinear ultrasonic detection of plasticity and fatigue. *J Acoust Soc Am* 2009;126(5). p. EL117-EL122.
- [35] Jingpin J, et al. Evaluation of the intergranular corrosion in austenitic stainless steel using collinear wave mixing method. *NDT and E Int* 2015;69:1–8.
- [36] Ju T, et al. Nondestructive evaluation of thermal aging of adhesive joints by using a nonlinear wave mixing technique. *NDT and E Int* 2019;103:62–7.
- [37] Hasanian M, Lissenden C. Second order ultrasonic guided wave mutual interactions in plate: Arbitrary angles, internal resonance, and finite interaction region. *J Appl Phys* 2018;124(16):164904.
- [38] Li W, et al. Theoretical analysis and experimental observation of frequency mixing response of ultrasonic Lamb waves. *J Appl Phys* 2018;124(4):044901.
- [39] Ishii Y, Biwa S, Adachi T. Non-collinear interaction of guided elastic waves in an isotropic plate. *J Sound Vib* 2018;419:390–404.
- [40] Jingpin J, et al. Nonlinear Lamb wave-mixing technique for micro-crack detection in plates. *NDT and E Int* 2017;85:63–71.
- [41] Metya A, Tarafder S, Balasubramaniam K. Nonlinear Lamb wave mixing for assessing localized deformation during creep. *NDT and E Int* 2018;98:89–94.
- [42] Pineda-Allen JC, Ng CT. Nonlinear Guided-Wave Mixing for Condition Monitoring of Bolted Joints. *Sensors* 2021;21(15):5093.
- [43] Shan S, et al. New nonlinear ultrasonic method for material characterization: Codirectional shear horizontal guided wave mixing in plate. *Ultrasonics* 2019;96:64–74.
- [44] Ding X, et al. One-way Lamb mixing method in thin plates with randomly distributed micro-cracks. *Int J Mech Sci* 2020;171:105371.
- [45] Sun M, Qu J. Analytical and numerical investigations of one-way mixing of Lamb waves in a thin plate. *Ultrasonics* 2020;108:106180.
- [46] Guan L, et al. Nonlinear Lamb Wave Micro-Crack Direction Identification in Plates with Mixed-Frequency Technique. *Appl Sci* 2020;10(6):2135.
- [47] Aslam M, Nagarajan P, Remanan M. Nonlinear ultrasonic evaluation of damaged concrete based on mixed harmonic generation. *Struct Control Health Monit* 2022;e3110.
- [48] Ng CT, Veidt M. A Lamb-wave-based technique for damage detection in composite laminates. *Smart Mater Struct* 2009;18(7):074006.
- [49] Guo N, Cawley P. The interaction of Lamb waves with delaminations in composite laminates. *J Acoust Soc Am* 1993;94(4):2240–6.
- [50] Ramadas C, et al. Interaction of the primary anti-symmetric Lamb mode (Ao) with symmetric delaminations: numerical and experimental studies. *Smart Mater Struct* 2009;18(8):085011.
- [51] Rajagopal P, et al. On the use of absorbing layers to simulate the propagation of elastic waves in unbounded isotropic media using commercially available Finite Element packages. *NDT and E Int* 2012;51:30–40.
- [52] Sampath S, Sohn H. Non-contact microcrack detection via nonlinear Lamb wave mixing and laser line arrays. *Int J Mech Sci* 2022;107769.
- [53] Sun M, et al. Experimental and numerical investigations of nonlinear interaction of counter-propagating Lamb waves. *Appl Phys Lett* 2019;114(1):011902.
- [54] Cho H, et al. Nonlinear guided wave technique for localized damage detection in plates with surface-bonded sensors to receive Lamb waves generated by shear-horizontal wave mixing. *NDT and E Int* 2019;102:35–46.
- [55] Pratt WK. Digital image processing. 4th ed. New York: Wiley-Interscience; 2001.
- [56] Kim J, et al. Experimental characterization of fatigue damage in a nickel-base superalloy using nonlinear ultrasonic waves. *J Acoust Soc Am* 2006;120(3):1266–73.
- [57] Zhu H, Ng CT, Kotousov A. Low-frequency Lamb wave mixing for fatigue damage evaluation using phase-reversal approach. *Ultrasonics* 2022;124:106768.
- [58] Ng CT, Yeung C, Yin T, He Y, Chen L. Investigation of nonlinear torsional guided wave mixing in pipes buried in soil. *Eng. Struct.* 2022;273:115089.
- [59] Ng CT, Yeung C, Yin T, Chen L. Stress evaluation of tubular structures using torsional guided wave mixing. *Smart Struct. Syst.* 2022;30(6):639–48.